JOURNAL OF AIRCRAFT
Vol. 42, No. 6, November–December 2005

Inverse Design of Adaptive Airfoils with Aircraft Performance Considerations

Jeffrey K. Jepson* and Ashok Gopalarathnam†
North Carolina State University, Raleigh, North Carolina 27695-7910

Recent advances in the development of inverse airfoil design methods now allow for the incorporation of aircraft performance considerations in the design of a nonflapped airfoil. Although these improvements make airfoil–aircraft matching considerably easier, there is a need for a similar capability for adaptive airfoils. A design formulation is presented that incorporates aircraft performance considerations in the inverse design of low-speed laminar-flow adaptive airfoils in which the adaptation is achieved using a trailing-edge cruise flap. The benefit of using adaptive airfoils is that the size of the low-drag region of the drag polar can be effectively increased without increasing the maximum thickness of the airfoil. Two aircraft performance parameters are considered: level-flight maximum speed and maximum range. It is shown that the lift coefficients for the lower and upper corners of the airfoil low-drag range can be appropriately adjusted to tailor the airfoil for these two aircraft performance parameters. The design problem is posed as a part of a multidimensional Newton iteration in an existing conformal-mapping-based inverse design code, PROFOIL. This formulation automatically adjusts the lift coefficients for the corners of the low-drag range for a given flap deflection as required for the airfoil–aircraft matching. Examples are presented to illustrate the flapped-airfoil design approach for a general aviation aircraft and the results are validated by comparison with results from postdesign aircraft performance computations.

Nomenclature

AR	=	wing aspect ratio
b	=	wingspan
C_D	=	aircraft or wing drag coefficient based on S_w
C_d	=	airfoil drag coefficient based on the chord
C_L	=	aircraft or wing lift coefficient based on S_w
C_l	=	airfoil lift coefficient based on the chord
C_m	=	airfoil pitching moment coefficient about the quarter-chord location
c	=	airfoil chord
e	=	Oswald's efficiency factor
M	=	Mach number
P_{av}	=	power available
P_{req}	=	power required
R	=	aircraft range
Re	=	Reynolds number
S	=	area
V	=	aircraft velocity
W	=	aircraft weight
W_e	=	aircraft weight without fuel
W_f	=	aircraft weight with fuel
α	=	angle of attack
α^*	=	design angle of attack for a segment
δ_f	=	flap angle
η_p	=	propeller efficiency
ρ	=	density

Subscripts

f	=	fuselage and other components of aircraft except wing
i	=	induced
ls	=	lower surface
max	=	maximum
min	=	minimum
p	=	profile
us	=	upper surface
w	=	wing
zl	=	zero lift

Superscripts

c	=	complex configuration
low	=	lower corner of the airfoil low-drag range
up	=	upper corner of the airfoil low-drag range

Presented as Paper 2004-0028 at the AIAA 42nd Aerospace Sciences Meeting, Reno, NV, 5–8 January 2004; received 12 July 2004; revision received 23 November 2004; accepted for publication 1 January 2005.

*Graduate Research Assistant, Box 7910, Department of Mechanical and Aerospace Engineering; jkjepson@eos.ncsu.edu. Student Member AIAA.

†Associate Professor, Box 7910, Department of Mechanical and Aerospace Engineering; ashok_g@ncsu.edu. Senior Member AIAA.

Introduction

OVER the past several decades, significant improvements have been made in the design of single-element airfoils. Early methods, such as those of Mangler[1] and Lighthill,[2] allowed for the prescription of the inviscid velocity distribution at a single operating condition. Since then, considerable strides have been made and it is now possible to design an airfoil using multipoint velocity distributions,[3] single-point boundary-layer specifications,[4] and simultaneous multipoint velocity and boundary-layer specifications.[5,6] Recent methods also allow for specifications of the laminar-to-turbulent transition curves[7] and design specifications that incorporate aircraft performance considerations such as level-flight maximum speed and maximum range.[8]

Although advances in single-element airfoil design methods have occurred steadily over the past 30 years, only recently has substantial progress been made in the development of inverse design methods for complex aerodynamic systems. Gopalarathnam and Selig[9] have developed a hybrid approach for the inverse design of complex aerodynamic systems such as flapped airfoils,[9] multi-element airfoils,[10,11] and airfoils for three-dimensional junctures.[12] The hybrid approach couples a conformal-mapping-based inverse design method with methods for analysis of the complex system and allows for multipoint velocity and boundary-layer specifications on the complex system.

The goal of the current research was to develop an inverse design method for adaptive airfoils that incorporates aircraft performance considerations from the outset in the design of airfoils with

trailing-edge "cruise" flaps. The use of a cruise flap allows an airfoil to be adapted to a wide range of lift coefficients. For this reason, natural laminar flow (NLF) airfoils with cruise flaps are widely used in high-performance sailplanes and have potential for use in general aviation aircraft and uninhabited aerial vehicles where good performance is important over a large speed range. This effort builds on the development of the hybrid inverse method[9] and the incorporation of aircraft performance considerations in the design of nonflapped airfoils.[8] The following section provides an overview of the design formulation. A more detailed description of the design method is then presented, followed by a description of the analysis tools used for validation. Finally, examples are presented that demonstrate the capabilities of the method and the benefits of using this design formulation for tailoring adaptive airfoils.

Overview of the Design Formulation

It is well understood that the low-drag region (LDR), or drag bucket, of an NLF airfoil can be shifted by the use of a trailing-edge flap, also known as a cruise flap.[13–16] Positive deflection of the cruise flap will cause the LDR to move to a higher C_l, whereas negative deflection will cause the LDR to move to a lower C_l. This trend can be seen in Fig. 1. In the figure, the drag polars for the NASA NLF(1)-0215F airfoil[15] with various flap deflections are shown along with the points corresponding to the upper and lower corners of the LDR. It is seen that, as the flap is deflected, the LDR moves to higher and lower C_l values, depending on flap deflection. Thus, an airfoil with a cruise flap is an adaptive airfoil. With recent interest in adaptive wing technology[17,18] and the recent development of sensing and automation schemes[16] for adaptive airfoils, it is of interest to develop efficient inverse design methods for such adaptive airfoils with cruise flaps.

As seen from Fig. 1, the movement of the LDR occurs along a curve, which can be straight or have a slight curvature depending on the airfoil. This trend was also shown to occur for changes to airfoil camber for nonflapped airfoils in Refs. 19 and 20. This "low-drag curve" is marked in Fig. 1. Of interest in the airfoil–aircraft design integration is the determination of values of the C_l on the low-drag curve at which the flapped-airfoil upper and lower corners need to be located for good performance at low and high speeds.

Because deflecting a cruise flap will move the LDR along the low-drag curve, cruise flaps can be used to effectively widen the LDR of the airfoil drag polar without increasing the thickness of the airfoil, which is useful when tailoring an airfoil for multiple aircraft performance parameters.

To provide an overview of the design formulation, the drag polar of an NLF airfoil is shown in Fig. 2. Also shown in the figure are the partial drag polars for the NLF airfoil with a 20%-chord cruise flap with $\delta_f = -5.0$ and 5.0 deg. The polars were obtained by analyzing the airfoil at a constant $Re\sqrt{C_l}$ to take into consideration the changes in Re that result from changes in airspeed associated with variations in the operating C_l for an aircraft in steady rectilinear flight. The C_l value for the upper corner of the LDR, C_l^{up}, for the airfoil with

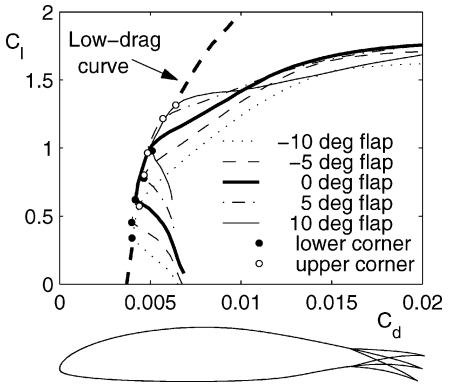

Fig. 1 Drag polars at a Reynolds number of 6×10^6 for the NASA NLF(1)-0215F airfoil with various flap deflections from XFOIL analysis.

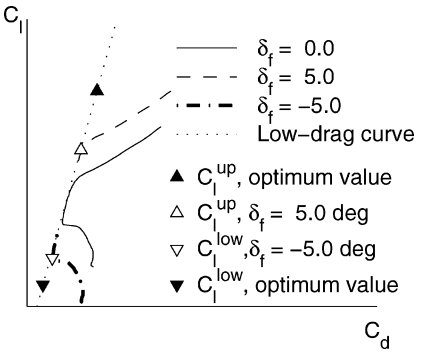

Fig. 2 Example airfoil drag polars with various values of δ_f used for illustration.

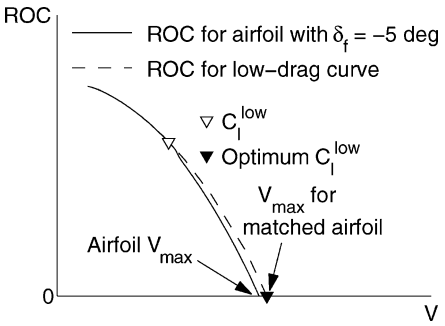

Fig. 3 Illustration of the effect of C_l^{low} on $V_{\max}$.

$\delta_f = 5.0$ deg and the C_l value for the lower corner of the LDR, C_l^{low}, with $\delta_f = -5.0$ deg are also shown in Fig. 2. Also shown in Fig. 2 is the low-drag curve. For a given flap defection, desired values for the upper and lower corners can be achieved by adjusting the airfoil camber and thickness as demonstrated in Ref. 19. It is not clear at the airfoil design stage, however, as to what are the most suitable values for C_l^{up} and C_l^{low} to match the airfoil to a given aircraft to maximize the performance of the aircraft.

Two aircraft performance parameters were considered in this study: level-flight maximum speed, $V_{\max}$, and maximum range, $R_{\max}$. Earlier work[8,20] demonstrated the suitability of the use of the two lift coefficients, C_l^{up} and C_l^{low}, as design variables to tailor an NLF airfoil for maximizing these two aircraft performance parameters. When tailoring an adaptive airfoil for these performance parameters for a given aircraft, the following questions can be posed

1) What is the best possible value for C_l^{low} with a specified negative flap deflection to tailor the airfoil for achieving the highest possible $V_{\max}$ without sacrificing low-speed performance?

2) What is the best possible value for C_l^{up} with a specified positive flap deflection to tailor the airfoil for the maximum-range condition without unnecessary penalties at the high-speed conditions?

The objective was to formulate the airfoil design problem so that airfoil–aircraft matching is achieved during the inverse airfoil design stages for adaptive airfoils.

It has been shown in Refs. 8 and 20 that, for nonflapped airfoils, the ideal value for C_l^{low} to achieve the maximum possible value of $V_{\max}$ occurs at a condition where the full-power aircraft rate of climb (ROC) is zero at $C_l = C_l^{\text{low}}$. This idea can be extended to flapped airfoils. Figure 3 shows the aircraft full-power ROC curve for the example NLF airfoil with a 20%-chord plain trailing-edge flap with $\delta_f = -5.0$ deg. The point corresponding to C_l^{low} is indicated in the figure. Also shown in this figure by a dashed line is the ROC variation for the airfoil drag variation that is represented by the low-drag curve in the C_d–C_l plot in Fig. 2—this ROC curve forms the envelope of ROC curves for the family of airfoils with a given amount of laminar flow, regardless of flap angle. The velocity corresponding to zero ROC is $V_{\max}$; the $V_{\max}$ values are marked in Fig. 3 for drag variations corresponding to the flapped airfoil and the low-drag curve. It is seen that, for the flapped airfoil used, $V_{\max}$ occurs when operating outside

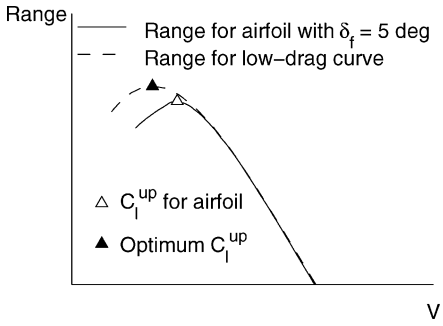

Fig. 4 Illustration of the effect of C_l^{up} on R_{max}.

the LDR; the C_l for V_{max} is less than C_l^{low}. Thus, the flapped airfoil can be better tailored for the V_{max} condition if C_l^{low} is decreased such that it corresponds to the C_l for V_{max}. This optimum value of C_l^{low} is the C_l value that corresponds to the V_{max} condition for the low-drag curve, shown as a downward, filled triangle in Figs. 2 and 3. This illustration provides useful guidelines for incorporating the airfoil–aircraft tailoring for the V_{max} condition in the inverse design process. A Newton iteration procedure can be used to adjust the design parameters that control C_l^{low} until C_l^{low} corresponds to the V_{max} condition, that is, until ROC $= 0$ at $C_l = C_l^{low}$.

Also shown in Refs. 8 and 20 is that the maximum aircraft range, R_{max} can be achieved by setting the value of C_l^{up} equal to the value of C_l on the low-drag curve that corresponds to R_{max}. This concept can also be used to tailor flapped airfoils. Figure 4 shows the variation of aircraft range, R, with velocity, V, for 1) the NLF airfoil with a 20%-chord plain trailing-edge flap deflected 5.0 deg as well as for 2) the low-drag curve. It is seen that C_l^{up} for the flapped airfoil, denoted by the upward open triangle symbol in Figs. 2 and 4, is less than the C_l corresponding to the R_{max} condition for the low-drag curve. This optimum value for C_l^{up} is denoted by the upward closed triangle symbols in Figs. 2 and 4. Therefore, when the flapped airfoil is tailored for the R_{max} operating condition of the aircraft, C_l^{up} will correspond to the optimum C_l for R_{max}. This matching can be achieved in the inverse design framework using Newton iteration to adjust the design variables that affect C_l^{up} until the difference between C_l^{up} and the optimum value for C_l^{up} is brought to zero.

Design Formulation

To incorporate aircraft performance considerations in the inverse design of adaptive airfoils, the inverse airfoil design method PROFOIL[5,6] was adapted. This section first briefly describes some of the main features of the PROFOIL code. The hybrid approach[9] used to design complex airfoil configurations in PROFOIL is also briefly discussed. The development of the design formulation to incorporate the two aircraft performance considerations (V_{max} and R_{max}) for adaptive airfoils is then presented.

Description of the PROFOIL Code

PROFOIL[5,6] is a multipoint inverse design method based on conformal mapping and builds on the theory of Eppler's inverse airfoil design approach.[3,21,22] In the method, the airfoil is divided into a finite number of segments each having a design angle of attack α^*, which is measured relative to α_{zl}. At the α^* for a segment, the velocity distribution over the segment is prescribed and can either be constant (as in Eppler's method[3]) or can have a nonlinear variation using a cubic-spline description.[6] Specifying α^* is equivalent to specifying a design value of C_l, C_l^*, because α^* is measured from the zero-lift line and the slope of the lift curve is approximately 2π per radian. In other words, the design lift coefficient for any segment is related to the segment α^* (in degrees) by:

$$C_l^* \approx 0.1 \times \alpha^* \tag{1}$$

In addition to single-element airfoils, PROFOIL has recently been extended for the design of complex airfoil configurations, such as multi-element and flapped airfoils, through the use of a hybrid approach[9] that couples the original single-element airfoil design method[5,6] with a two-dimensional panel method, PAN2D.[9] In the approach, conformal mapping is used to design the isolated airfoils and the panel method is then used to analyze the resulting complex airfoil configuration at the user-specified operating point, C_l^c. The design variables associated with the conformal-mapping inverse technique are then automatically adjusted to achieve desired aerodynamic specifications on the complex configuration.

PROFOIL can also solve for the boundary-layer development along the surface of the airfoil at a specified C_l on a single-element airfoil or at a specified C_l^c on a complex airfoil configuration using a direct integral method. Using the inviscid velocity distribution, PROFOIL can calculate boundary-layer properties such as shape factor H_{12} and transition amplification factor n. Because this boundary-layer calculation is intended to be used as a part of the rapid, interactive inverse method, the simple integral boundary-layer method has two restrictions: 1) it is valid only for attached boundary layers and 2) no viscous–inviscid interactions are considered. In other words, the inviscid pressure distribution is not adjusted to account for the effects of the boundary-layer displacement thickness. The n development is calculated using Drela's approximate e^n method.[23,24] In the current work, transition is assumed to occur when n equals a user-specified critical value of n_{crit} or when laminar separation is encountered. This assumption is valid for flows in which transition is caused by the amplification of Tollmien–Schlichting waves and for airfoils that do not have significant laminar separation bubbles.

In the current approach to airfoil–aircraft matching, there is a need to determine the airfoil C_d for a given δ_f at specified values of C_l within the drag bucket several times during the inverse design process. A procedure was developed for determining an approximate but rapid estimate for the airfoil C_d within the PROFOIL code. The assumption in the approximate method is that the pressure-drag contributions can be neglected when estimating airfoil C_d for C_l values that lie within or at the corners of the low-drag range. In the approach developed in this research, the airfoil C_d is computed at a given C_l by first using the airfoil inviscid velocity distribution along with the direct integral boundary-layer method in PROFOIL to determine the locations of the upper- and lower-surface transition of the laminar boundary layer. The skin-friction drag coefficient is then estimated using flat-plate boundary-layer equations from Ref. 25 for the known extents of laminar and turbulent boundary layers on both surfaces of the airfoil. The reason for using the flat-plate equations for determining the skin-friction C_d of the airfoil is that the integral boundary-layer method in PROFOIL is not valid for separated boundary layers. Although the final airfoil is not expected to have a separated boundary layer when operating within the low-drag range, there is a possibility that intermediate airfoils generated during the Newton iteration process could have trailing-edge separation. Therefore, to have a robust iteration procedure, the flat-plate equations for known transition locations were used in the iteration process for determining the skin-friction C_d.

Figure 5 shows a comparison between the skin-friction C_d calculated using this approximate approach and the total airfoil C_d

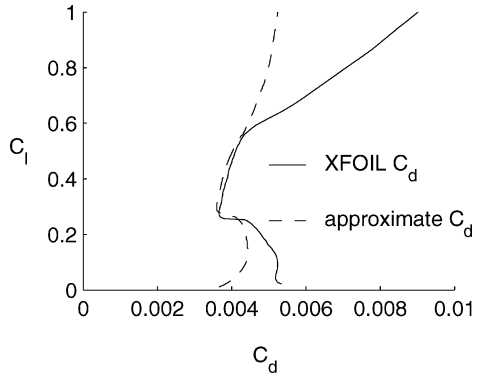

Fig. 5 Comparison between the skin-friction C_d from the current method and total C_d from XFOIL at $Re\sqrt{C_l} = 3.42 \times 10^6$.

obtained from XFOIL[23] analysis, which computes both the skin-friction and pressure contributions to airfoil C_d. It can be seen that the skin-friction C_d closely corresponds to the total airfoil C_d at C_l values within the drag bucket. This approximate method of determining the airfoil C_d was developed to obtain rapid estimates suitable for the potentially large number of C_d evaluations that could be required during inverse design.

One of the main features of PROFOIL is a multidimensional Newton iteration scheme that allows for the prescription of several aerodynamic and geometric characteristics. This multidimensional Newton iteration scheme is utilized in the current work to incorporate the aircraft $V_{\max}$ and $R_{\max}$ design considerations. In this scheme, control over some of the parameters used in the conformal mapping is given up to achieve the desired specifications. These parameters are altered via the Newton iteration until the desired specifications are satisfied.

Flapped Airfoil Tailoring for $V_{\max}$

As illustrated earlier in Fig. 3, an airfoil with a flap deflected upward and tailored for the aircraft $V_{\max}$ condition will have ROC = 0 at the level-flight speed corresponding to C_l^{low}. To examine how to incorporate this specification in the inverse-design Newton iteration structure, it is necessary to first examine the contribution of the airfoil C_d to the aircraft ROC. With the assumption that, at any given C_L, the wing profile drag coefficient is equal to the airfoil C_d, the aircraft C_D can be determined by adding the wing C_{D_i} and the parasite-drag contribution of the fuselage and other components to the wing profile drag coefficient:

$$C_D = C_d + C_{Df} S_f / S_w + C_L^2 \big/ \pi e \mathrm{AR} \tag{2}$$

The resulting aircraft drag, power required for level flight, and ROC can then be determined as follows:

$$D = \frac{1}{2}\rho V^2 (C_d S_w + C_{Df} S_f) + \frac{2W^2}{\pi b^2 e \rho V^2} \tag{3}$$

$$P_{\text{req}} = \frac{1}{2}\rho V^3 (C_d S_w + C_{Df} S_f) + \frac{2W^2}{\pi b^2 e \rho V} \tag{4}$$

$$\text{ROC} = \eta_p P_{\text{av}} - P_{\text{req}} \tag{5}$$

Another important element of the overall scheme is the capability to generate an airfoil that achieves a desired value of C_l^{low} when the flap is deflected to a specified angle. The details of this capability and the hybrid design approach are documented in Ref. 9. A brief illustration is provided here using an example airfoil for which the desired C_l^{low} is 0.2 when the 20%-chord trailing-edge flap is deflected to −5 deg. For this design problem, the velocity distribution on a large segment on the lower surface, shown in the geometry plot in Fig. 6a, at the α^* for the segment is defined using spline support points. Using the multidimensional Newton iteration, this velocity distribution is varied to achieve a desired variation in the lower-surface transition amplification factor n at $C_l = 0.2$ and at the appropriate Reynolds number when $\delta_f = -5$ deg.

Figure 6b shows the desired transition amplification factor at this condition, as well as the resulting n development that satisfies the specification. Such an n-development prescription ensures that, while the lower surface has laminar flow to at least $0.5c$ with $\delta_f = -5$ deg at a C_l of 0.2 and higher, this laminar boundary layer is on the verge of transition at this condition. Any reduction in C_l below 0.2 for the −5-deg flap case will result in a rapid forward movement of the lower-surface transition location. In effect, this prescription allows anchoring of the lower corner of the low-drag

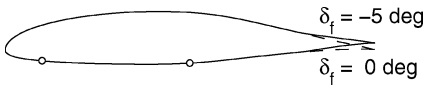

Fig. 6a Geometry for the example airfoil for the 0-deg and −5-deg flap settings (with the design segment endpoints marked).

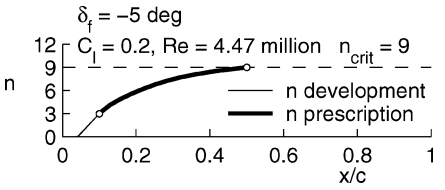

Fig. 6b *n* development on the lower surface for the −5-deg flap setting as computed by PROFOIL compared with the prescription.

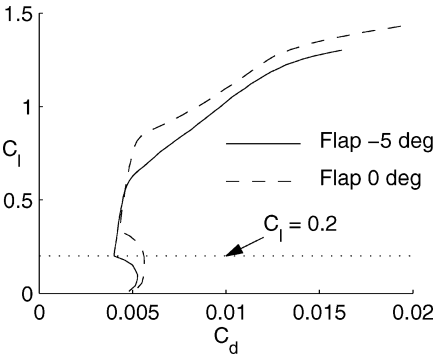

Fig. 6c Drag polars for the example airfoil for 0-deg and −5-deg flap settings.

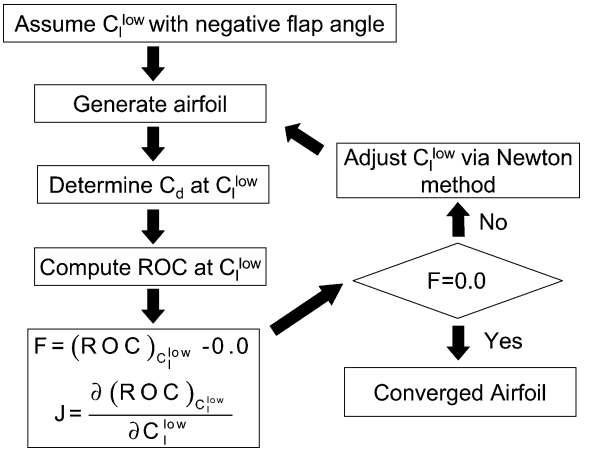

Fig. 7 Flow chart for $V_{\max}$ tailoring.

range at the desired C_l^{low} when the flap is deflected to the specified angle. Figure 6c shows the drag polars for the unflapped and the flapped airfoils for this example and clearly shows that C_l^{low} for the airfoil generated using the approach is 0.2 when $\delta_f = -5$ deg, as desired. When the desired C_l^{low} is altered during the Newton iteration, it is also necessary to alter α^* for the segments on the lower surface by 1 deg for every 0.1 change in C_l^{low}, as suggested by Eq. (1).

A flowchart of the overall scheme for $V_{\max}$ tailoring is shown in Fig. 7. The first step in the $V_{\max}$ tailoring process is to assume a starting value of C_l^{low} for a specified negative flap deflection and to generate the airfoil. The flapped-airfoil C_d at this C_l^{low} is determined using the approximate skin-friction estimate. For this operating lift coefficient and the corresponding flight velocity, the resulting ROC is determined using Eqs. (2–5). Once the ROC at C_l^{low} with the flap deflection is known, the corresponding element of the residual vector can be calculated using the following equation:

$$F = (\text{ROC})_{C_l^{\text{low}}} - 0.0 \tag{6}$$

The Jacobian is calculated using a finite difference approach by calculating the change in ROC at C_l^{low} due to a small perturbation

to C_l^{low}:

$$J = \frac{\partial(\text{ROC})_{C_l^{\text{low}}}}{\partial C_l^{\text{low}}} \tag{7}$$

If the residual is not zero, C_l^{low} is adjusted and the iteration is continued until the ROC at C_l^{low} is zero.

Thus, by posing the design problem as a part of the Newton iteration framework, the inverse method can be used to determine the optimum value of C_l^{low} for a given aircraft–engine–propeller combination and to determine the corresponding airfoil shape at the user-specified δ_f.

Flapped Airfoil Tailoring for $R_{\max}$

An airfoil with a flap deflected downward and tailored for the maximum-range flight condition needs to have C_l^{up} be equal to the optimum C_l^{up}, as illustrated in Fig. 4. The range, R, at any given C_l is given by the well-known Bréguet range equation:

$$R = \frac{\eta}{\text{SFC}} \frac{C_L}{C_D} \int_{W_e}^{W_f} \frac{\mathrm{d}W}{W} \tag{8}$$

Figure 8 shows the basic procedure used to tailor a flapped airfoil for $R_{\max}$. The first step is to design an initial or starting airfoil. Once the airfoil is designed, the value of C_l^{up} can be obtained. However, the determination of the value of C_l^{up} within the PROFOIL code is not straightforward. Unlike with the lower surface, the values of α^* for the segments on the upper surface vary significantly from the leading edge to the trailing edge.[19] For this reason, C_l^{up} for the initial airfoil with the user-specified flap deflection is determined by generating a drag polar for the flapped airfoil using XFOIL. For the determination of optimum C_l^{up}, $(C_l^{\text{up}})_{\text{opt}}$, a linearized approximation to the equation for the low-drag curve is obtained by use of finite differencing to determine the change in airfoil skin-friction C_d for a given change in C_l^{up}. This equation for the low-drag curve is updated at every step in the Newton iteration. The optimum C_l^{up} is determined by finding the C_l value along the linearized low-drag curve that gives the maximum aircraft range. For each C_l analyzed, the aircraft velocity is determined and the aircraft range is then calculated using Eqs. (2) and (8). Once the values for both C_l^{up} and $(C_l^{\text{up}})_{\text{opt}}$ are determined, the elements of the residual and Jacobian can be calculated using the following equations:

$$F = C_l^{\text{up}} - \left(C_l^{\text{up}}\right)_{\text{opt}} \tag{9}$$

$$J = \frac{\partial C_l^{\text{up}}}{\partial \alpha_{\text{us}}^*} \tag{10}$$

The Jacobian is calculated in the same manner as it was calculated for the $V_{\max}$ tailoring. The difference is that the α^* values for the segments on the upper surface, denoted by α_{us}^*, are used as the design variables in this case. Once the elements of the residual and Jacobian are calculated, the α_{us}^* values are adjusted in the Newton iteration process and the airfoil is redesigned. As the α^* values for the upper-surface segments are altered, the value of C_l^{up} is adjusted accordingly using a gradient of 0.1 change in C_l^{up} for every degree change in the upper-surface α^*. This process continues until the value of C_l^{up} equals $(C_l^{\text{up}})_{\text{opt}}$.

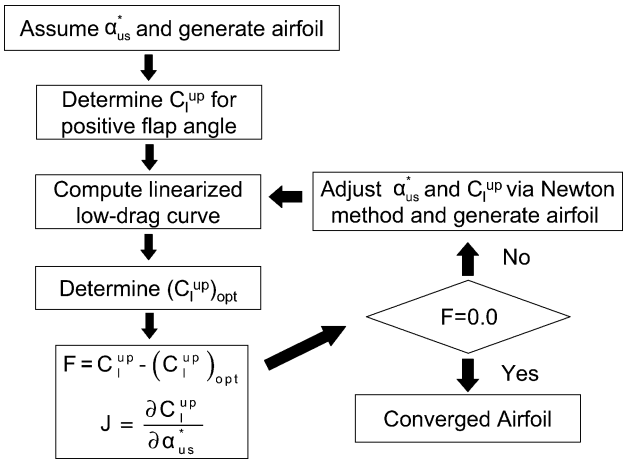

Fig. 8 Flow chart for $R_{\max}$ tailoring.

The use of such approximations in C_l and C_d in the design formulation enables rapid design via the Newton iteration process. It must be mentioned that the objectives in the design formulation are only to determine the best values for C_l^{up} and C_l^{low} and not to predict the resulting values of $V_{\max}$ and $R_{\max}$. For these objectives, the approximations are not only valid, but also enable rapid, interactive design.

The aforementioned procedure describes the use of multidimensional Newton iteration to simultaneously tailor a flapped airfoil for both the $V_{\max}$ and $R_{\max}$ conditions by adjusting the design variables that control C_l^{low} and C_l^{up}, each with the appropriate flap angle. In doing so, the airfoil maximum camber and thickness ratios are determined by the design method. Tailoring for the $V_{\max}$ and $R_{\max}$ conditions implies that the airfoil can operate in the LDR for a wide range of flight speeds with the appropriate flap deflection. It is noted, however, that this procedure is one of many possibilities for posing the airfoil design problem. As an alternate example, one could tailor the airfoil for just the $V_{\max}$ condition and specify the thickness ratio without tailoring the airfoil for the $R_{\max}$ condition. Also, for some design scenarios, it may be desirable to tailor the airfoil for maximum aircraft endurance, rather than $R_{\max}$, by using the Bréguet endurance equation instead of Eq. (8).

Although the procedure outlined in this paper focuses on the tailoring of flapped airfoils using the PROFOIL inverse design method, it is conceivable that the overall ideas outlined in the paper can be used in other direct design methods in which the airfoil geometry parameters form the design variables. For example, it may be possible to use Newton iteration to adjust the airfoil maximum camber and thickness ratios in a direct design method to tailor for the $V_{\max}$ and $R_{\max}$ conditions with appropriate flap angles. However, because the connections between the design variables and the final airfoil performance are typically weaker for direct design approaches than for inverse design approaches, it may be necessary to run XFOIL or a similar analysis method in the iteration loop when using a direct design approach.

Analysis Tools for Validation

This section describes the tools and methodology used to validate the results obtained using the PROFOIL code. The approach used for the validation is similar to that used in Ref. 8 for nonflapped airfoils. The first step in the validation approach was to analyze the converged airfoil using the XFOIL code[23] to calculate the drag polar of the airfoil to take into consideration both the pressure and skin-friction contributions to the airfoil C_d.

Once the airfoil drag polar was calculated, the WINGS code[20] was used to calculate the trimmed induced and profile drag of the lifting surfaces of the aircraft. WINGS is a vortex lattice code that can handle multiple lifting surfaces. The code reads in the XFOIL α–C_l–C_d–C_m polar output files to allow for the use of the airfoil drag polar and pitching moment curves for various sections along the wing and horizontal tail. In the current analysis, the incidence of the horizontal tail at each angle of attack is adjusted to trim the aircraft (i.e., to set $C_{M_{\text{c.g}}} = 0.0$). As a consequence, the aircraft performance estimates take into account the trimmed drag contributions associated with changes to the wing airfoil $C_{M_{c/4}}$ that accompany changes to the airfoil camber and flap angle.

After the total drag of the aircraft is calculated, the performance of the aircraft was calculated using PERF.[20] PERF is an aircraft performance simulation code that uses the equations discussed in the preceding section along with the drag output from the WINGS code to calculate the aircraft ROC and range at each angle of attack. This postdesign approach was used to generate all of the performance plots to validate the results obtained from the inverse design method.

Table 1 Assumed geometry, drag, and power characteristics for the hypothetical general aviation airplane

Parameter	Value
Gross weight (W)	14269 N (3200 lbf)
Wing reference area (S_w)	9.10 m^2 (97.92 ft^2)
Wing aspect ratio (AR)	9.1
Equivalent parasite drag area of airplane minus wing ($C_{Df}S_f$)	0.1647 m^2 (1.772 ft^2)
Rated engine power (P_{av})	261 kW (350 hp)
Specific fuel consumption (SFC)	8.31×10^{-7} N/s/W (0.5 lbf/h/hp)
Fuel volume	341 l (90 gal)

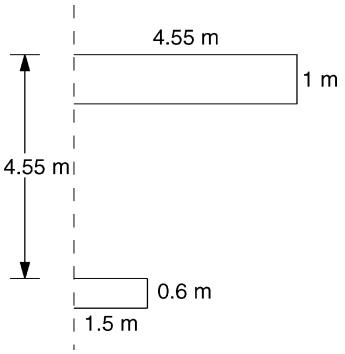

Fig. 9 Planview showing the right-side geometry of the wing and tail for the hypothetical aircraft.

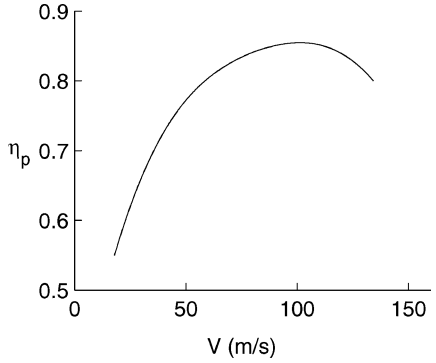

Fig. 10 Assumed propeller-efficiency distribution.

Aircraft Specification

This section presents the relevant details of a hypothetical general aviation aircraft used in the rest of the paper. The aircraft, used earlier in Ref. 8, is a conventional, aft-tail configuration with a constant-speed propeller driven by a piston engine. The planview of the wing and tail of the aircraft is shown in Fig. 9.

Table 1 provides the relevant specifications for the aircraft. As shown, an equivalent parasite drag area ($C_{Df}S_f$) has been assumed for the fuselage and all the components of the airplane except the wing. The propeller efficiency was assumed to have the nonlinear variation with velocity shown in Fig. 10. The static margin for the hypothetical aircraft was assumed to be 15% of the wing mean aerodynamic chord.

Demonstration of the Design Method

Because airplanes operate at several operating conditions, it is desirable to design an airfoil that is tailored for a range of flight conditions. Two ways of achieving this tailoring within the PROFOIL inverse design code are by using either the design method described in Ref. 8 for nonflapped airfoils or the current method for adaptive airfoils. The use of an adaptive airfoil is particularly useful when the airfoil is designed for extensive laminar flow as will be shown in the following examples.

In the first example, the method for nonflapped airfoils in Ref. 8 was used to tailor an airfoil to maximize both V_{max} and R_{max} for the general aviation aircraft shown earlier in Fig. 9. The airfoil was

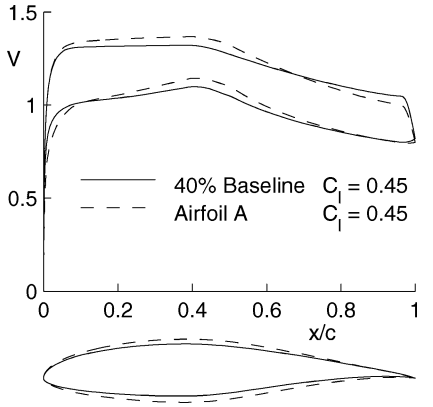

Fig. 11 Geometries and inviscid velocity distributions for the 40%c laminar flow baseline airfoil and converged airfoil A.

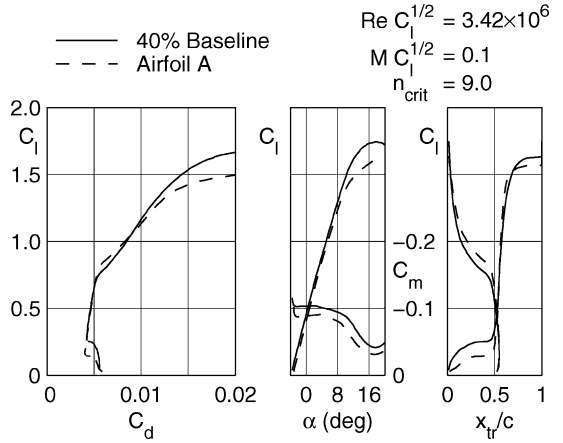

Fig. 12 Polars for the 40%c laminar flow baseline airfoil and the converged airfoil A from XFOIL analysis.

designed for a reduced Reynolds number, $Re\sqrt{C_l}$, of 3.42 million. This reduced Reynolds number corresponds to rectilinear flight at standard sea-level conditions for the aircraft. The airfoil was also designed to support approximately 40%c laminar flow on the upper and lower surfaces when operating in the LDR. The thickness-to-chord ratio of the baseline airfoil used as a starting point for the design was specified to be 14%c. With this starting airfoil, a new nonflapped airfoil was designed and was tailored for both V_{max} and R_{max} aircraft operating conditions. The performance specifications were achieved by adjusting the α^* values for the lower surface to satisfy the V_{max} requirements while also adjusting the α^* values for the upper surface to satisfy the R_{max} specifications.

The geometry for the baseline airfoil and the converged airfoil (labeled A) are shown in Fig. 11. Because both the specifications were being satisfied, the thickness ratio was left unspecified and was determined by the method. The thickness ratio increased to 17%c as a result of the tailoring. The drag polars for the baseline and converged airfoils are shown in Fig 12. It can be seen that airfoil A has the optimized values of $C_l^{low} = 0.16$ and $C_l^{up} = 0.82$. Figures 13 and 14 show the ROC and range variations for the baseline and converged airfoil A. It can be seen from the figures that converged airfoil A has a small improvement in both V_{max} and R_{max} over the baseline airfoil.

Although the first example showed that it is possible to successfully tailor an airfoil with 40%c laminar flow for both V_{max} and R_{max} without using a flap, a designer may want to reduce the drag of the airfoil by increasing the extent of laminar flow on the airfoil. One consequence of increasing the amount of laminar flow while maintaining the airfoil maximum thickness ratio is that the size of the drag bucket decreases. As a result, the thickness of the tailored airfoil will increase when tailoring an airfoil with significant laminar flow

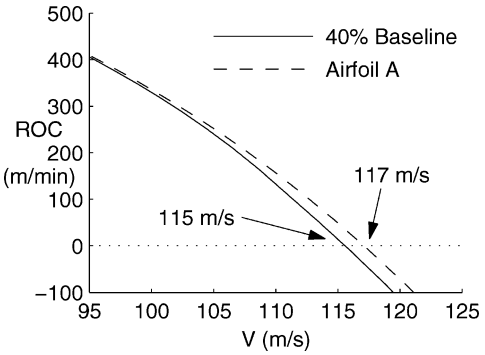

Fig. 13 ROC curves for the 40%c laminar flow baseline airfoil and airfoil A.

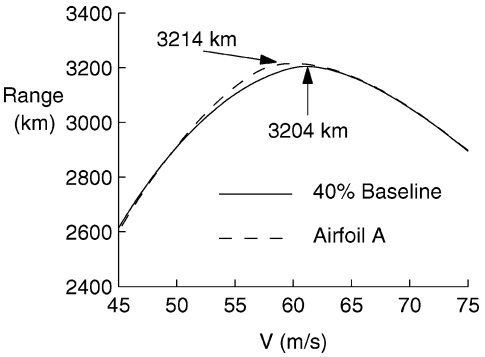

Fig. 14 Range curves for the 40%c laminar flow baseline airfoil and airfoil A.

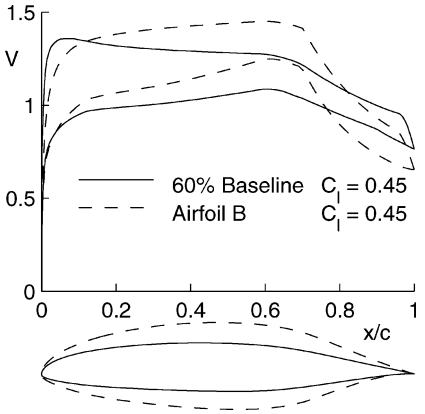

Fig. 15 Geometries and inviscid velocity distributions for the 60%c laminar flow baseline airfoil and the converged airfoil B.

for both $V_{\max}$ and $R_{\max}$ conditions. To demonstrate this result, an NLF airfoil with 60%c laminar flow was tailored for both $V_{\max}$ and $R_{\max}$. A baseline airfoil of 14%c thickness and 60%c laminar flow was designed for this example. Figure 15 shows the airfoil shape as well as the inviscid velocity distributions for the baseline airfoil and converged airfoil B. As in the preceding example, the thickness of the converged airfoil was determined as an output of the method. As a result of the tailoring for both $V_{\max}$ and $R_{\max}$ conditions, the thickness ratio increased to 25%c. This undesirably large increase in thickness can lead to separated flow on the airfoil and large pressure drag. The large thickness ratio can be avoided by the use of an adaptive airfoil.

In the next example, the 60%c laminar flow baseline airfoil was again used as a starting point and an adaptive airfoil with a 10%c cruise flap was designed so that $V_{\max}$ is optimized when $\delta_f = -5.0$ deg and $R_{\max}$ is optimized when $\delta_f = 10.0$ deg. This matching was achieved in PROFOIL by adjusting the α^* values on the lower surface to satisfy the $V_{\max}$ condition with $\delta_f = -5.0$ deg

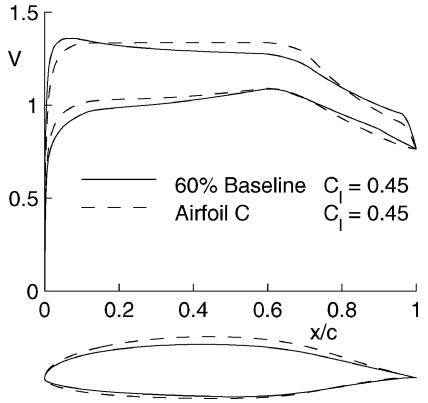

Fig. 16 Geometries and inviscid velocity distributions for the 60%c laminar flow baseline airfoil and the converged airfoil C.

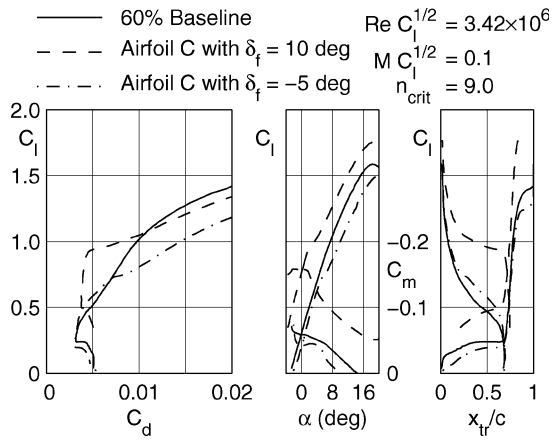

Fig. 17 Polars for the 60%c laminar flow baseline airfoil and airfoil C with $\delta_f = -5.0$ and 10.0 deg from XFOIL analysis.

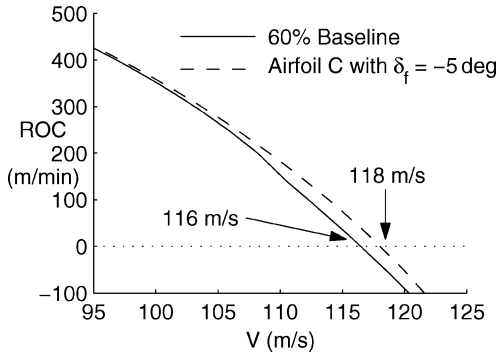

Fig. 18 ROC curves for the 60%c laminar flow baseline airfoil and airfoil C with $\delta_f = -5.0$ deg.

while simultaneously adjusting the α^* values on the upper surface to satisfy the $R_{\max}$ condition with $\delta_f = 10.0$ deg. As in the preceding examples, the thickness ratio was left unspecified because both specifications were being made simultaneously. As a result of the specifications, the thickness ratio increased to 16.7%c, which is quite acceptable. The geometry and inviscid velocity distributions for the 60%c laminar flow baseline airfoil and the converged airfoil (labeled C) are shown in Fig. 16. The drag polars for the 60%c laminar flow baseline airfoil and airfoil C with flap deflected -5 and 10 deg are shown in Fig 17. It is seen that airfoil C has $C_l^{\text{low}} = 0.21$ with $\delta_f = -5.0$ deg and $C_l^{\text{up}} = 0.91$ with $\delta_f = 10.0$ deg.

The ROC curves for the 60%c laminar flow baseline airfoil and for airfoil C with $\delta_f = -5.0$ deg are shown in Fig. 18. As the figure demonstrates, when the flap is deflected to -5.0 deg, the improvement in $V_{\max}$ over the 60%c laminar flow baseline airfoil

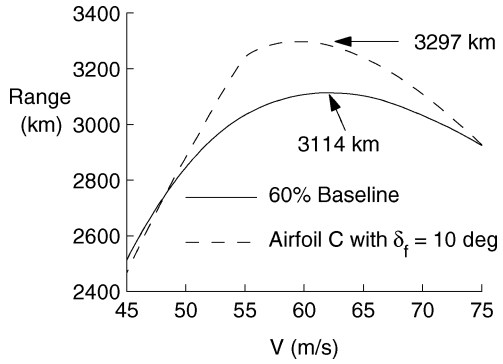

Fig. 19 Range curves for the 60%c laminar flow baseline airfoil and airfoil C with $\delta_f = 10.0$ deg.

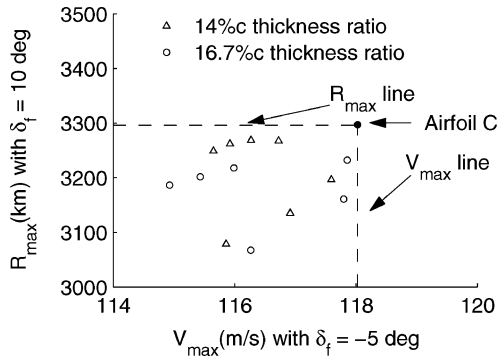

Fig. 20 $R_{\max}$ with $\delta_f = 10.0$ deg vs $V_{\max}$ with $\delta_f = -5.0$ deg for several airfoils with 60%c laminar flow.

is similar to that achieved by airfoil A over the 40%c laminar flow baseline airfoil shown earlier in Fig. 13. Figure 19 shows the range curves for the baseline airfoil as well as for airfoil C with flap deflected 10.0 deg. As the figure shows, airfoil C with $\delta_f = 10.0$ deg achieves a greater improvement in $R_{\max}$ over the 60%c laminar flow baseline airfoil than airfoil A does over the 40%c laminar flow baseline airfoil, shown earlier in Fig. 14. However, airfoil C achieves higher values of both $V_{\max}$ and $R_{\max}$ than does airfoil A because of the increased extents of laminar flow. These results further demonstrate that a flapped airfoil can be tailored for both $V_{\max}$ and $R_{\max}$ conditions using the current method.

Although airfoil C produces a higher $V_{\max}$ with $\delta_f = -5.0$ deg and a higher $R_{\max}$ with $\delta_f = 10.0$ deg than the $V_{\max}$ and $R_{\max}$ of the baseline airfoil, it is unclear whether or not airfoil C achieves the maximum values of $V_{\max}$ and $R_{\max}$. To examine this further, several airfoils were designed with 60%c laminar flow and various amounts of camber. The airfoils were designed to have two different thickness ratios, either the baseline 14%c or the tailored 16.7%c. The airfoils were analyzed using XFOIL with a 10%c flap deflected −5.0 and 10.0 deg. For each of the airfoils designed, the values of $R_{\max}$ with $\delta_f = 10.0$ deg and $V_{\max}$ with $\delta_f = -5.0$ deg were determined using the validation approach discussed earlier. Figure 20 shows the results from this analysis as well as the values of $V_{\max}$ and $R_{\max}$ for the converged airfoil C, marked with a filled circle. The results for the 14%c airfoil are marked with upward pointing triangles whereas the 16.7%c results are marked with open circles. It is seen that the converged airfoil has the highest values of both $R_{\max}$ and $V_{\max}$. This postdesign study demonstrates that the design formulation successfully tailors the airfoil for both $V_{\max}$ and $R_{\max}$ flight conditions with flap deflection.

Conclusions

Recent advances in inverse airfoil design methods enabled the incorporation of aircraft performance considerations in the design of nonflapped airfoils. Although these enhancements have made airfoil–aircraft matching considerably easier, the thickness of an airfoil can increase dramatically when it is tailored for more than one performance consideration. This is especially true of airfoils with large amounts of laminar flow. This large thickness ratio can be avoided by using an adaptive airfoil. The advantage of using adaptive airfoils is that the size of the drag bucket can be effectively increased without increasing the thickness. The objective of the current method was to incorporate aircraft performance considerations in the inverse design of adaptive airfoils with cruise flaps. Two aircraft performance parameters have been considered: level-flight maximum speed and maximum range. The design problem is then posed in the form of two questions:

1) What is the optimum lift coefficient for the lower corner of the airfoil drag polar to tailor the airfoil for the aircraft level-flight maximum speed condition for a given negative flap deflection?

2) What is the optimum lift coefficient for the upper corner of the airfoil drag polar to tailor the airfoil for the maximum range flight condition for a given positive flap deflection?

This paper presents a design formulation that allows for the incorporation of these design considerations in a multidimensional Newton iteration framework available in the PROFOIL inverse airfoil design code. In this Newton iteration process, the conformal-mapping variables that control the lift coefficients for the upper and lower corners of the airfoil drag bucket are automatically adjusted to tailor the airfoil for one or both of these two aircraft flight conditions, each with a given flap deflection. As a result, the airfoil lower-surface aerodynamics is tailored so that the aircraft ROC is zero when the airfoil is operating at the lower corner of the low-drag range with a negative flap deflection and likewise the airfoil upper-surface aerodynamics is tailored for the maximum-range flight condition with a positive flap deflection. The use of the approximate drag model within the Newton iteration ensures that the inverse design procedure is computationally efficient, often converging within a couple of minutes. The results of the inverse design have been validated in the paper by postdesign studies using aircraft performance computations. By utilizing adaptive airfoils, the current design formulation allows a designer to tailor an airfoil with large amounts of laminar flow for multiple aircraft performance considerations while maintaining a reasonable airfoil thickness.

Acknowledgments

This research was supported by a grant from the National Institute of Aerospace. The support is gratefully acknowledged.

References

[1]Mangler, W., "Die Berechnung eines Tragflugelprofiles mit vorgeschreibener Druckverteilung," *Jahrbuch der deutschen Luftfahrtforschung*, Vol. 1, Air Ministry of London Translation No. 932, 1940, pp. 46–53.

[2]Lighthill, M. J., "A New Method of Two-Dimensional Aerodynamic Design," Aeronautical Research Council, R&M 2112, April 1945.

[3]Eppler, R., and Somers, D. M., "A Computer Program for the Design and Analysis of Low-Speed Airfoils," NASA TM 80210, Aug. 1980.

[4]Henderson, M. L., "Inverse Boundary-Layer Technique for Airfoil Design," *Advanced Technology Airfoil Research*, Vol. 1, NASA CP-2045, Pt. 1, March 1978, pp. 383–397.

[5]Selig, M. S., and Maughmer, M. D., "A Multi-Point Inverse Airfoil Design Method Based on Conformal Mapping," *AIAA Journal*, Vol. 30, No. 5, 1992, pp. 1162–1170.

[6]Selig, M. S., and Maughmer, M. D., "Generalized Multipoint Inverse Airfoil Design," *AIAA Journal*, Vol. 30, No. 11, 1992, pp. 2618–2625.

[7]Jepson, J. K., and Gopalarathnam, A., "Inverse Airfoil Design via Specification of the Boundary-Layer Transition Curve," AIAA Paper 2003-0212, Jan. 2003.

[8]Jepson, J. K., and Gopalarathnam, A., "Incorporation of Aircraft Performance Considerations in Inverse Airfoil Design," *Journal of Aircraft*, Vol. 42, No. 1, 2005, pp. 199–207.

[9]Gopalarathnam, A., and Selig, M. S., "A Hybrid Approach to Inverse Design of Complex Aerodynamic Systems," AIAA Paper 2000-0784, Jan. 2000.

[10]Gopalarathnam, A., and Selig, M. S., "Multipoint Inverse Method for Multielement Airfoil Design," *Journal of Aircraft*, Vol. 35, No. 3, 1998, pp. 398–404.

[11]Gopalarathnam, A., and Selig, M. S., "A Multipoint Viscous Design Method for Multi-Element Airfoils," AIAA Paper 98-2404, June 1998.

[12]Gopalarathnam, A., and Selig, M. S., "Hybrid Inverse Airfoil Design Method for Complex Three-Dimensional Lifting Surfaces," *Journal of Aircraft*, Vol. 39, No. 3, 2002, pp. 409–417.

[13]Pfenninger, W., "Investigation on Reductions of Friction on Wings, in Particular by Means of Boundary Layer Suction," NACA TM 1181, Aug. 1947.

[14]McGhee, R. J., Viken, J. K., Pfenninger, W., Beasley, W. D., and Harvey, W. D., "Experimental Results for a Flapped Natural-Laminar-Flow Airfoil with High Lift/Drag Ratio," NASA TM 85788, May 1984.

[15]Somers, D. M., "Design and Experimental Results for a Flapped Natural-Laminar-Flow Airfoil for General Aviation Applications," NASA TP 1865, June 1981.

[16]McAvoy, C. W., and Gopalarathnam, A., "Automated Cruise Flap for Airfoil Drag Reduction over a Large Lift Range," *Journal of Aircraft*, Vol. 39, No. 6, 2002, pp. 981–988.

[17]Stanewsky, E., "Aerodynamic Benefits of Adaptive Wing Technology," *Aerospace Science and Technology*, Vol. 4, No. 7, 2000, pp. 439–452.

[18]Monner, H. P., Breitbach, E., Bein, T., and Hanselka, H., "Design Aspects of the Adaptive Wing—The Elastic Trailing Edge and the Local Spoiler Bump," *Aeronautical Journal*, Vol. 104, Feb. 2000, pp. 89–95.

[19]Gopalarathnam, A., and Selig, M. S., "Low-Speed Natural-Laminar-Flow Airfoils: Case Study in Inverse Airfoil Design," *Journal of Aircraft*, Vol. 38, No. 1, 2001, pp. 57–63.

[20]Gopalarathnam, A., and McAvoy, C. W., "Effect of Airfoil Characteristics on Aircraft Performance," *Journal of Aircraft*, Vol. 39, No. 3, 2002, pp. 427–433.

[21]Eppler, R., "Direkte Berechnungvon Tragflugelprofilen aus der Druckverteilung," *Ingenieur-Archive*, Vol. 25, No. 1, 1957, pp. 32–57; transl. "Direct Calculation of Airfoil from Pressure Distribution," NASA TT F-15, 417, 1974.

[22]Eppler, R., *Airfoil Design and Data*, Springer-Verlag, New York, 1990.

[23]Drela, M., "XFOIL: An Analysis and Design System for Low Reynolds Number Airfoils," *Low Reynolds Number Aerodynamics*, edited by T. J. Mueller, Lecture Notes in Engineering, Vol. 54, Springer-Verlag, New York, 1989, pp. 1–12.

[24]Drela, M., and Giles, M. B., "Viscous-Inviscid Analysis of Transonic and Low Reynolds Number Airfoils," *AIAA Journal*, Vol. 25, No. 10, 1987, pp. 1347–1355.

[25]Houghton, E. L., and Carpenter, P., *Aerodynamics for Engineering Students*, Wiley, New York, 1993, p. 373.